

## Energy dependence of $T_{20}$ and $\tau_{21}$ in $\pi d$ elastic scattering

G. R. Smith, D. R. Gill, D. Healey, D. Ottewell, G. D. Wait, and P. Walden  
*TRIUMF, Vancouver, British Columbia, Canada V6T 2A3*

R. R. Johnson, G. Jones, R. Olszewski, F. M. Rozon, R. Rui,\*  
 M. E. Sevier, and R. P. Trelle  
*University of British Columbia, Vancouver, British Columbia, Canada V6T 1W5*

E. L. Mathie, G. Lolos, S. I. H. Naqvi, and V. Pafilis  
*University of Regina, Regina, Saskatchewan, Canada S4S 0A2*

N. R. Stevenson and R. B. Schubank  
*University of Saskatchewan, Saskatoon, Saskatchewan, Canada S7N 0W0*

W. Gyles and C. R. Ottermann  
*Kernforschungszentrum Karlsruhe, Institut für Kernphysik and Institute für Experimentelle Kernphysik  
 der Universität Karlsruhe, 7500 Karlsruhe, Federal Republic of Germany*

G. S. Kyle

*New Mexico State University, Las Cruces, New Mexico, 88003*

(Received 29 February 1988)

Angular distributions of the tensor analyzing powers  $T_{20}$  and  $\tau_{21}$  have been measured for  $\pi d$  elastic scattering, in a single scattering experiment employing a tensor polarized deuteron target. Measurements of  $T_{20}$  were obtained for pion bombarding energies of 134, 151, 180, 220, and 256 MeV. Measurements of  $\tau_{21}$  were obtained for pion bombarding energies of 134, 180, and 220 MeV. The results are compared with three-body calculations where effects relating to pion absorption are seen to play an important role.

### I. INTRODUCTION

The study of the  $\pi d$  elastic scattering reaction is of fundamental importance in intermediate energy pion physics. The deuteron is the simplest real nucleus which can be studied with pions, and forms our basis for understanding more complicated systems on a microscopic level. It is the only system which can, in principle, be calculated exactly, using three-body theories with measured  $\pi N$  and  $NN$  phases as input.<sup>1-17</sup> The more advanced of these theories are unified in the sense that they address the  $\pi NN$  system as a whole. The reaction channels  $\pi d \rightarrow \pi d$ ,  $\pi d \leftrightarrow NN$ ,  $\pi d \rightarrow \pi NN$ ,  $NN \rightarrow \pi NN$ , and  $NN \rightarrow NN$  are all considered to be coupled together. The simultaneous prediction of many observables for all these channels provides a severe constraint on the theory. It is, therefore, a goal of the experimentalist to provide as broad and diverse a data base as possible with which to confront the theory. Spin observables may provide a relatively sensitive testing ground in this respect due to their sensitivity to the interference of small amplitudes with the larger ones which dominate spin averaged observables like the differential cross section. The detailed comparison of the predicted and measured behavior of spin observables provides one of our best opportunities for understanding the physics of the elastic scattering process,

including the weak, second-order processes which contribute to it.

Additional insight to the underlying physics of the  $\pi NN$  system may also be obtained from a direct comparison of the theoretically predicted amplitudes to those which arise from a fit to measured data in a partial wave analysis.<sup>18-20</sup> The central quantities of a theoretical prediction are, after all, not the observables themselves but rather the amplitudes. These amplitudes may be experimentally determined without ambiguity if the data forming the basis of the fit are complete. For the case of the  $\pi d$  elastic channel, four complex spin amplitudes are required to describe the scattering, which means that, in principle, seven observables need to be measured at each energy and at each scattering angle in order to determine the amplitudes up to a common phase. In practice, this infinite basis is usually truncated by expressing the amplitudes as partial waves. Only a few partial waves are required at energies spanning the (3,3) resonance region. However, measurements of spin observables, and at least two spin transfer observables for the same angular and incident energy regime, are deemed essential for an unambiguous analysis.

In spite of the above points, experimental studies of  $\pi d$  elastic scattering in the (3,3) resonance region have been limited until recently to measurements of the differential

cross section, probably the least sensitive observable of all. The most precise measurements of the differential cross section for  $\pi d$  elastic scattering have been reported in Ref. 21 at forward angles, and in Ref. 22 at backward angles, with good agreement in the regions of overlap. However, problems arise in predicting the behavior of even this relatively insensitive observable at backward angles. These problems are still with us today.

There are four independent spin observables in the  $\pi d$  elastic channel: The vector analyzing power  $iT_{11}$ , and the tensor analyzing powers  $T_{20}$ ,  $T_{21}$ , and  $T_{22}$ . One of these, the vector analyzing power  $iT_{11}$ , has been thoroughly studied at intermediate energies. The initial measurements of this observable, first reported in 1981 and 1982, were sparse and of poor quality.<sup>23</sup> Progress in the techniques of polarizing deuteron targets, coupled with superior experimental techniques geared specifically for the measurements of  $\pi d$  observables, resulted in a much improved and more comprehensive set of measurements of  $iT_{11}$  (Ref. 24) reported in 1984. A subset of these latter data was compared to three-body Faddeev calculations at the canonical bombarding energies of 140, 180, 220, 256, and 294 MeV. The result was that the conventional calculations failed to describe the measured  $iT_{11}$  at each energy, the failure becoming more acute at higher energies and at forward angles. Qualitative agreement with the measured values of  $iT_{11}$  could only be achieved by reducing the impact of pion absorption via the  $P_{11}$   $\pi N$  partial wave input, although this simultaneously worsened the agreement with the differential cross sections.

The first measurement of a tensor observable, the tensor polarization  $t_{20}$ , was reported in 1979.<sup>25</sup> This initial measurement was confined to  $180^\circ$  at a single bombarding energy (142 MeV). More or less the same experimental group went on to publish the first (three point) angular distribution of  $t_{20}$  in 1981.<sup>26</sup> These measurements employed an unpolarized deuteron target and a deuteron polarimeter to measure the tensor polarization  $t_{20}$  of the recoil deuteron in  $\pi d$  elastic scattering. These initial measurements were also found to be in disagreement with the three-body calculations available at the time. The failure of the conventional calculations persisted at higher energies, which were studied subsequently<sup>27</sup> by the same experimental group. Although their measurements of  $t_{20}$  were confined to only two or three angles at 180, 220, and 256 MeV, they underscored the importance of true pion absorption. Whereas the full calculations failed to describe the limited data at each of the bombarding energies studied, calculations without true pion absorption were in closer qualitative agreement with the data.

In the meantime (1982), measurements of  $t_{20}$  were reported<sup>28</sup> by a different group at another laboratory, but for a similar bombarding energy (134 MeV) and at similar angles. The experimental technique employed for this experiment was also similar to that of Refs. 25, 26, and 27 in that for both experiments recoil deuterons from  $\pi d$  elastic scattering using a deuteron polarimeter based on the  ${}^3\text{He}(d,p){}^4\text{He}$  reaction. The results of the two experi-

ments were, however, in strong disagreement with each other. These new data generated considerable interest in the community, not only because of the inconsistency of the new results with the previous measurements, but because the results of Ref. 28 were cited as evidence for dibaryon resonances.

Both groups repeated and extended their measurements, each confirming their own results. A third group, which again used a  ${}^3\text{He}$  polarimeter for the recoil deuterons in order to measure  $t_{20}$  in a double scattering, reported their results<sup>29</sup> in 1985 which were consistent with the earlier measurements of Ref. 26.

Finally, in 1986, measurements of the tensor analyzing power  $T_{20}$  were reported at bombarding energies of 134 and 151 MeV.<sup>30</sup> This experiment employed a tensor polarized deuteron target in a single scattering experiment (no polarimeter was thus required). As the experimental technique was completely different from that employed in the double scattering measurements, the results could be used to settle the controversy surrounding the measurements of  $t_{20}$  once and for all. The results were in agreement with those of Refs. 25, 26, 27, and 29, effectively ruling out those of Ref. 28. Furthermore, they supported the growing body of evidence that pion absorption was being treated incorrectly in the three-body calculations. Again, qualitative agreement with experiment was found only for those calculations in which the  $P_{11}$  (pion absorption) contribution was removed. On the other hand, the limited energy regime of the  $T_{20}$  measurements of Ref. 30 left open the question of whether there was a systematic problem with the theory. In particular, large differences between calculations with and without pion absorption are predicted at higher ( $T_\pi > 180$  MeV) bombarding energies.

Measurements of the tensor analyzing power,  $\tau_{21}$  were first reported in 1987 at 180 MeV.<sup>31</sup> The technique used was similar to that used successfully for the measurement of  $T_{20}$ .<sup>30</sup> The  $T_{20}$  data, and the surviving  $t_{20}$  data,<sup>25,26,27,29</sup> all pointed to the failure of the full three-body calculation in conjunction with the relative success of the same model when pion absorption was removed from the calculations. The predictions of  $\tau_{21}$  at 180 MeV were consistent with the measured values regardless of whether pion absorption was included or not. It is, therefore, important to find out whether the predicted differences between the  $\tau_{21}$  calculations with and without pion absorption, which become significant at bombarding energies other than 180 MeV, are confirmed by experiment.

As we have pointed out, in principle there are two techniques for measuring spin observables in  $\pi d$  scattering. One involves measuring the polarization of recoil deuterons with a  ${}^3\text{He}$  polarimeter in a second scattering. Such experiments usually employ (unpolarized) liquid deuterium targets. Clearly, the double-scattering technique is a difficult one, a fact which is underscored by the measurements of Ref. 28 which employed this technique and which were shown to be erroneous. Furthermore, the double-scattering technique suffers from low counting rates, so that a systematic measurement including many scattering angles and bombarding energies would con-

sume an extraordinary amount of experimental running time. Finally, as discussed later, measurements of  $t_{20}$  in a double-scattering experiment are not clean in the sense that what is really measured is a mixture of  $T_{20}$ ,  $T_{21}$ , and  $T_{22}$ . Therefore, we have chosen to measure the  $\pi d$  spin observables in a single-scattering experiment, using a tensor polarized deuteron target. Such a configuration has been shown to be a reliable, efficient method for measurements of this type.<sup>24,30,31</sup>

In this article we report the energy dependence of  $T_{20}$  and  $\tau_{21}$  measured for  $\pi d$  elastic scattering using a tensor polarized deuteron target. New results for  $T_{20}$  are reported for bombarding energies of 180, 220, and 256 MeV. New results for  $\tau_{21}$  are reported for bombarding energies of 134 and 220 MeV. Our earlier results at 134 and 151 MeV ( $T_{20}$ ) (Ref. 30) and 180 MeV ( $\tau_{21}$ ) (Ref. 31) are also included here for completeness. Since this concludes the main portion of our program of measuring spin observables in the  $\pi d$  elastic channel at TRIUMF, we report as well the details of our experimental technique. In the following section (Sec. II) we summarize the formalism which leads to expressions for the tensor analyzing powers. Then, in Sec. III we discuss the experimental technique used for the measurements. The tensor polarized deuteron target is discussed in detail in Sec. IV. The results of this experiment are presented in Sec. V, followed by a discussion of the theoretical analysis in Sec. VI. A summary of the conclusions drawn from these measurements can be found in Sec. VII.

## II. FORMALISM

Before describing the experiment or the results it is necessary to define the observables of interest,  $T_{20}$  and  $\tau_{21}$ , in terms of the quantities actually measured during the experiment. In doing so we must reconcile the two coordinate systems which present themselves in a natural way. One coordinate system is defined in terms of the incident and scattered pion trajectories (the scattering plane) and is used to describe differential cross sections. The other deals with the target polarization and is referred to the spin alignment axis of the target deuterons, which is, of course, coincident with the target magnetic field axis. In accordance with the usual Madison convention,<sup>32</sup> we adopt the former reference frame which necessitates a rotation of the target polarization into the coordinate frame of the scattering.<sup>33</sup>

The coordinate frame of the scattering is one in which the  $z$  axis lies along the incident pion momentum, and the  $y$  axis is perpendicular to the scattering plane defined by the incident and scattered pion momenta. The dependence of the differential cross section  $\sigma(\text{pol})$  for scattering from a polarized target may be expressed in terms of the cross section  $\sigma(\text{unp})$  for scattering from an unpolarized target, and all independent spin observables  $T_{kq}$  according to<sup>32,33</sup>

$$\sigma(\text{pol}) = \sigma(\text{unp}) (1 + a_{11} iT_{11} + a_{20} T_{20} + a_{21} T_{21} + a_{22} T_{22}), \quad (1)$$

where

$$a_{11} = \sqrt{3} p_z \sin \alpha \cos \beta,$$

$$a_{20} = \frac{p_{zz}}{\sqrt{2}} \frac{3 \cos^2 \alpha - 1}{2},$$

$$a_{21} = \sqrt{3} p_{zz} \sin \alpha \cos \alpha \sin \beta,$$

and

$$a_{22} = -\frac{\sqrt{3}}{2} p_{zz} \sin^2 \alpha \cos 2\beta.$$

The target vector (tensor) polarization is denoted by  $p_z$  ( $p_{zz}$ ) in the coefficients  $a_{kq}$  above. The Euler angles  $\alpha$  and  $\beta$ , which appear in Eq. (1), refer, respectively, to the polar angle between the incident pion beam and the target magnetic field, and the angle between the  $y$  axis and the projection of the target magnetic field on the  $x$ - $y$  plane. For reference, the coordinate system is presented in Fig. 1.

The deuteron has spin 1, and consequently has three magnetic substates,  $m = \pm 1, 0$ . Denoting the population of these substates by  $n^+$ ,  $n^-$ , and  $n^0$ , the vector polarization of the target can be expressed as

$$p_z = \frac{n^+ - n^-}{n^+ + n^- + n^0}$$

and the tensor polarization as

$$p_{zz} = \frac{n^+ + n^- - 2n^0}{n^+ + n^- + n^0} = \frac{1 - 3n^0}{n^+ + n^- + n^0},$$

where use had been made of the normalization

$$n^+ + n^- + n^0 = 1.$$

From these expressions (ignoring contributions from the deuteron quadrupole moment), the magnitude of target tensor polarization can be derived from the vector polarization according to

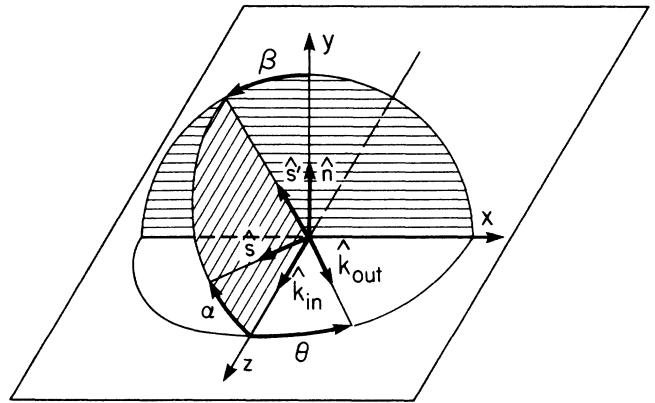


FIG. 1. The coordinate system used for the definition of the Euler angles  $\alpha$  and  $\beta$  is shown. The pion beam is incident along  $\hat{k}_{in}$  and the scattered pion trajectory is along  $\hat{k}_{out}$ . The spin alignment axis is coincident with the target magnetic field axis, denoted by  $\hat{S}$ .

$$p_{zz} = 2 - (4 - 3p_z^2)^{1/2}, \quad (2)$$

assuming the populations of the magnetic substates are described by a Maxwell-Boltzmann distribution.

Measurement of a given spin observable  $T_{kq}$  is accomplished by choosing appropriate values of  $\alpha$  and  $\beta$  such that the contribution of other spin observables is eliminated or minimized. Measurements of  $T_{20}$  are performed in an experimental configuration such that  $\alpha$  is  $0^\circ$ . This implies the target magnetic field axis is aligned along the incident beam direction (longitudinally). With  $\alpha = 0^\circ$ , the contribution to Eq. (1) from the other  $T_{kq}$  is zero, since they all involve a factor of  $\sin\alpha$ . The result is a clean, simple expression for  $T_{20}$  which involves only the polarized and unpolarized  $\pi d$  elastic cross sections and the target tensor polarization according to

$$T_{20} = \frac{\sqrt{2}}{p_{zz}} \left[ \frac{\sigma(\text{pol})}{\sigma(\text{unp})} - 1 \right]. \quad (3)$$

In order to emphasize the spin observable  $T_{21}$ , the appropriate choices of  $\alpha$  and  $\beta$  are  $\alpha = 57.3^\circ$  (to eliminate the  $T_{20}$  term) and  $\beta = 90^\circ$  (to eliminate the  $iT_{11}$  term). Unfortunately, the geometry of the polarized deuteron target is such that the angular region (in the horizontal plane) from  $50^\circ$  to  $78^\circ$  and from  $102^\circ$  to  $130^\circ$  is inaccessible. Therefore, for purely experimental reasons,  $\alpha$  was chosen to be  $45^\circ$  for the  $T_{21}$  measurements, and  $\beta$ ,  $90^\circ$ . In terms of the experimental configuration, this implies that the target magnetic field is oriented in the horizontal plane, at an angle of  $45^\circ$  to the incident beam. With these choices for  $\alpha$  and  $\beta$ , Eq. 1 can be written as

$$\tau_{21} \equiv T_{21} + \frac{1}{2} \left[ \frac{T_{20}}{\sqrt{6}} + T_{22} \right] \quad (4)$$

$$= \frac{2}{\sqrt{3}p_{zz}} \left[ \frac{\sigma(\text{pol})}{\sigma(\text{unp})} - 1 \right]. \quad (5)$$

The experimentally measured quantities are the target tensor polarization,  $p_{zz}$ , and the relative  $\pi d$  elastic scattering differential cross sections  $\sigma(\text{pol})$  and  $\sigma(\text{unp})$ . The quantity in parentheses in Eq. (4) is what is actually measured in a  $T_{22}$  experiment.<sup>34</sup> In a  $T_{21}$  experiment the quantity actually measured is a mixture of  $T_{21}$ ,  $T_{20}$ , and  $T_{22}$  according to Eq. (4), which we refer to as  $\tau_{21}$ . The dominant contribution to  $\tau_{21}$  comes from  $T_{21}$  since the  $T_{20}$  term is weighted by  $1/(2\sqrt{6})$  and the  $T_{22}$  term, weighted by a factor of  $\frac{1}{2}$ , is predicted to be small in the backward hemisphere where this experiment was performed.<sup>1-16</sup>

We have chosen to present our results as the specific linear combination of tensor observables given by Eq. (4) because this linear combination can be expressed entirely in terms of the experimentally measured quantities given by Eq. (5). Our experimental results for  $\tau_{21}$  are thus independent of calculated values for  $T_{20}$  and  $T_{22}$ . When comparing these results to calculations, however, the predictions for  $T_{20}$ ,  $T_{21}$ , and  $T_{22}$  must be combined according to Eq. (4).

Each of the (c.m.) spin observables has definite bounds.<sup>35</sup> These are  $0 \leq |it_{11}| \leq \sqrt{3}/2$ ,  $-\sqrt{2} \leq t_{20} \leq 1/\sqrt{2}$ , and  $0 \leq |t_{21}| \leq \sqrt{3}/2$ .

### III. EXPERIMENTAL TECHNIQUE

The detection system used for the  $T_{20}$  measurements is shown in Fig. 2. The experimental layout for the  $\tau_{21}$  measurements was similar, except that the entire target assembly and the detectors were rotated  $45^\circ$  to the left, looking downstream (along the incident beam direction). The main characteristics of the detection system are as follows: A solid angle of 27 msr for each of six independent arms ( $i=1,6$ ) was defined by a pion scintillator ( $\pi 2_i$ ) located 1 m from the polarized target, of dimensions  $9.0 \times 30.0 \text{ cm}^2$ . Together with another scintillator ( $\pi 1_i$ ) at 0.5 m radius with dimensions  $4.9 \times 16.5 \text{ cm}^2$ , this constituted one of six pion telescopes. Each of the pion scintillators was 3.1 mm thick.

Each pion telescope was placed in coincidence with an associated recoil deuteron arm consisting of three scintillators. The first scintillator ( $D1_i$ ) at a radius of 1.3 m from the target was a thin (3.2 mm) scintillator of dimensions  $9.0 \times 40.0 \text{ cm}^2$  which provided time-of-flight (TOF) as well as energy loss ( $\Delta E$ ) information. Following this scintillator was an aluminum absorber whose thickness was adjusted so that deuterons stopped in the following 1.27 cm thick scintillator ( $D2_i$ ) of dimensions  $9.0 \times 41.0 \text{ cm}^2$ . The third was a veto scintillator ( $D3_i$ ) of dimensions  $9.0 \times 41.0 \text{ cm}^2$  and 6.4 mm thick.

The flux of the incident beam was counted directly with scintillators S1 and S2 in coincidence, each of

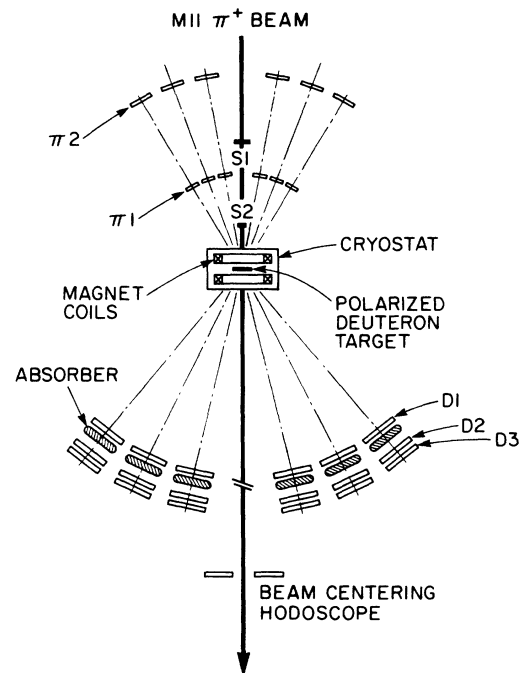


FIG. 2. The experimental layout is shown with the pion beam incident from the top. The meaning of the various detector rings is explained in the text.

which was 1.6 mm thick. The size of  $S2$  was chosen such that its image at the target would be smaller than the target itself. Protons in the incident beam were reduced by using a differential degrader (2 mm) near the midplane of the  $M11$  channel. Those remaining in the beam were eliminated by placing pulse height requirements on  $S1$  and  $S2$  in the trigger, defined by

$$S1 \cdot S2 \cdot \overline{S1} \cdot \overline{S2} \cdot \pi_{1_i} \cdot \pi_{2_i} \cdot D1_i \cdot \overline{D3_i} .$$

The incident flux was typically  $2 \times 10^6 \pi^+$  /sec. The position of the target within the cryostat was verified with x-ray pictures. The horizontal divergence of the beam was less than one degree. The vertical divergence of the beam was also constrained to less than  $1^\circ$  by the vertical dimension of the in-beam scintillator  $S2$ . The incident beam energies in this experiment were  $178.8 \pm 0.5$ ,  $218.6 \pm 0.5$ , and  $254.3 \pm 0.5$  MeV for the  $T_{20}$  measurements, and  $134.0 \pm 0.5$  and  $220.0 \pm 0.5$  MeV for the  $T_{21}$  measurements. The momentum acceptance of the  $M11$  channel corresponding to each of these bombarding energies was, respectively,  $\Delta p/p = \pm 2.2\% \pm 2.2\%$ ,  $\pm 5.0\% \pm 1.7\%$ , and  $\pm 1.1\%$ .

Clearly, the polarizing magnetic field influenced the trajectories of the particles. In each case the target was polarized at a field of 2.5 T. The magnitude of the target magnetic field was kept fixed at 2.5 T for the  $T_{20}$  measurements, and at 1.25 T for the  $\tau_{21}$  measurements. In other words, the target was operated in a frozen spin configuration for the  $\tau_{21}$  measurements in order to reduce the deflection of the scattered pions. The deflection is worse for the  $\tau_{21}$  measurements because the magnetic

field is oriented at  $45^\circ$  to the incident beam in this case. For the  $T_{20}$  measurements, the pion trajectories were more nearly parallel to the magnetic field of the target with correspondingly less deflection.

Each pion telescope was tilted and raised or lowered vertically to correspond to the actual pion trajectories deflected through the magnetic field of the polarized target. The pion trajectories were calculated using the calculated magnet field distribution of the polarized target, and the kinematics for  $\pi d$  scattering, taking into account the associated recoil deuteron angle. The angle subtended by the target magnetic field axis relative to the incident beam direction was carefully set to within  $\pm 0.5^\circ$  in an alignment procedure in the experimental area using measurements of the target magnetic field at a series of points in space downstream of the target. A specially designed compass was constructed for these measurements which measured the direction of the magnetic field over a planar region of space approximately 5 cm on a side. Separate measurements were performed to determine the angle of the magnetic field lines in both the horizontal and vertical planes. A series of such measurements was made in horizontal lines extending from 20 to 150 cm from the polarized target location in steps of a few centimeters. This series was repeated above, below, to the left, and to the right of the nominal magnetic field axis. The entire collection of measurements was then analyzed to determine the actual direction of the magnetic field axis. If the resulting magnetic field axis was more than  $0.5^\circ$  from the incident beam direction, the entire polarized target assembly was rotated accordingly, and the measurements described earlier were repeated as a check.

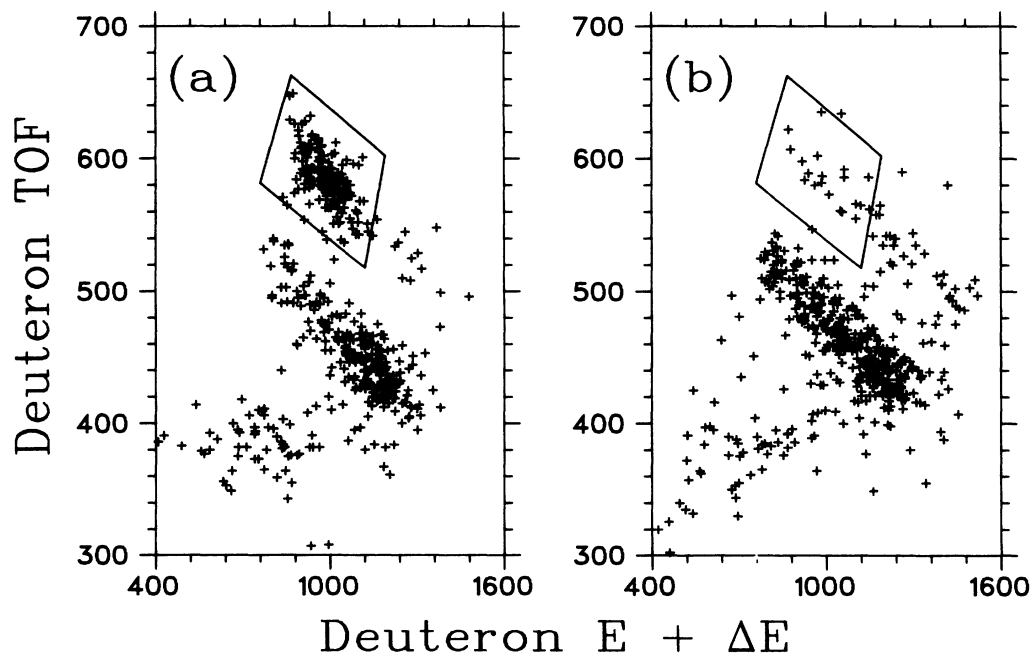


FIG. 3. A typical two-dimensional spectrum for the (a) foreground and (b) background targets is shown. The vertical axis is the deuteron TOF, and the horizontal axis is the sum of the deuteron pulse heights in the  $\Delta E$  counter ( $D1$ ) and the  $E$  counter ( $D2$ ). This example is for  $T_\pi = 180$  MeV and  $\theta_{c.m.} = 140^\circ$ . The region corresponding to  $\pi d$  elastic scattering is enclosed by the polygon. The other events are from quasielastic scattering, absorption, and deuteron breakup reactions.

The final analysis of the data was performed by constructing polygons around the  $\pi d$  elastic events identified in two-dimensional histograms of the deuteron TOF versus the deuteron total energy  $E + \Delta E$ , where  $\Delta E$  corresponded to the pulse height in  $D1$ , and  $E$  to the pulse height in  $D2$ . The resulting scatterplot provides good particle identification and clearly separates deuterons from protons. A typical (foreground) scatterplot of these quantities is shown in Fig. 3(a). The effect of placing various filters on the events was also investigated during the analysis of the data. In particular, software filters were used to select pions in the pion telescopes using the energy loss and TOF information available. Similar filters were placed on the deuteron telescopes to select deuterons. Scatterplots were made using deuteron TOF information from a hardware meantimer, as well as a software meantimer (employing TOF information from the tubes on opposite ends of the  $D1_i$  scintillators). Whereas the effect of the various filters was pronounced for the background quasi-free  $\pi p$  and absorption events, there was little impact in the region of the deuteron events in the scatterplots typified by Fig. 3. Since in these scatterplots the deuteron events are already cleanly separated from the quasi-free  $\pi p$  and absorption events, no filters were used in the final analysis of the data.

Explicit measurements of the background arising from quasi-elastic  $\pi d$  scattering from the contaminant carbon and oxygen nuclei in the polarized target material were also made by replacing the deuterated butanol target with an equivalent amount of nondeuterated butanol ( $C_4H_9OH$ ). The presence of hydrogen in the background target presented no problem as the experimental configuration provided excellent particle identification in the recoil deuteron (proton) detectors. These background measurements were made once at the end of each experimental running period, for each of the angles for which foreground data were acquired. The resulting yield was subtracted from the foreground yield to obtain background free results. The background amounted to 5% of the foreground, typically, in the region of the  $\pi d$  elastic scattering events [see Fig. 3(b)].

The uncertainty in the final results includes the statistical uncertainties in the relative cross sections (typically 1%), as well as an uncertainty associated with the relative measurement of  $p_{zz}$ , typically 5% (relative). An overall normalization uncertainty of 5% (relative), arising from the systematic uncertainty in calibrating the absolute target polarization, is included in the quoted uncertainties for  $T_{20}$  and  $\tau_{21}$ .

#### IV. POLARIZED TARGET

The tensor polarized target consisted of  $2.4 \text{ cm}^3$  of frozen 1 mm diameter beads contained in a thin walled teflon basket measuring  $22 \times 18 \times 6 \text{ mm}^3$ . The beads were composed of a mixture of 95% fully deuterated *N*-butyl alcohol ( $C_4D_9OD$ ) and 5%  $D_2O$  into which deuterated EHBA- $Cr^{III}$  (Ref. 36) was dissolved to a molecular density of  $6 \times 10^{19}$  atoms/ml. The packing density of the butanol beads was approximately 0.7. The teflon basket, which also served as a support for an NMR pickup coil, was im-

mersed in a mixture of  $^3He/^4He$  in the mixing chamber of a dilution refrigerator.

Microwaves used for the dynamic polarization of the target were provided by a 100 mW IMPATT source capable of delivering frequencies between 69 and 72 GHz. As the target polarization increased, the microwave power to the target microwave cavity was gradually lowered from 2 to 0.25 mW. The frequency delivered was stabilized by computer feedback to a tolerance of 1 MHz.

The polarizing field of 2.5 T was provided by two superconducting coils in the "thick" Helmholtz configuration with a horizontal magnetic field axis either  $0^\circ$  (for the  $T_{20}$  measurements) or  $45^\circ$  (for the  $\tau_{21}$  measurements) to the incident beam axis. This alignment was carefully checked to within  $0.5^\circ$  by means of a series of magnetic field measurements at various points in space downstream of the polarized target, described earlier. The  $\tau_{21}$  data were acquired with the target in frozen spin mode at a holding field of 1.25 T. The  $T_{20}$  data were acquired with the target magnetic field at 2.5 T. The target tensor polarizations achieved in this experiment varied from run to run, from  $0.10 \pm 0.005$  to  $0.17 \pm 0.009$ .

The magnitude of target polarization was determined from measurements of the deuteron NMR signal. The NMR pickup coil consisted of a 48 turn coil of 0.1 mm

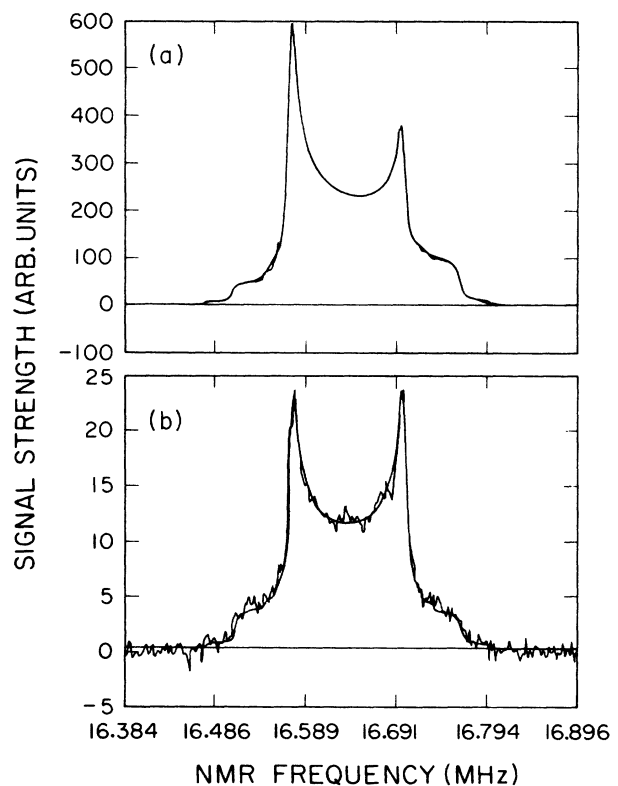


FIG. 4. (a) Typical dynamically polarized and (b) thermal equilibrium deuteron NMR signals are shown. The polarizations corresponding to these signals are 0.47 (dynamically polarized) and 0.00053 (thermal equilibrium). The solid line going through the data is a fit using a theoretical lineshape described in Ref. 38.

diameter copper wire which surrounded the target material. During the course of these experiments, two NMR systems were employed. The first system<sup>37</sup> employed an NMR circuit which was kept at resonance at all times. The most stable results were obtained using a design which removed all active electronics from the refrigerator and measured the rf NMR signals at the end of a  $\lambda/2$  cable. The  $Q$  curve was cancelled with an equivalent tuned circuit at room temperature. The real part of the NMR signal was measured using a synchronous detector.

The target polarization was obtained from analysis of the NMR signals using two independent techniques, the thermal equilibrium (TE) technique and the asymmetry technique. Both techniques rely on the relationship between  $p_z$  and  $p_{zz}$  given by Eq. 2. The deuteron NMR signal has a complicated shape due to the interaction of the deuteron quadrupole moment and the electric field gradient in the butanol molecule. The result is a signal consisting of two partially overlapping, asymmetric peaks in the NMR frequency spectrum. In fact, there are even two more smaller peaks which arise from the OD bonds in butanol (and  $D_2O$ ), but which are hard to see in the NMR spectrum due to the predominance of the transitions arising from the CD bonds. A typical dynamically polarized deuteron NMR signal is plotted in Fig. 4(a).

The TE technique involves comparing the total area of the dynamically polarized deuteron NMR signal with the total area of the TE NMR signal. The TE polarization can be deduced from the known values of temperature and magnetic field, assuming a Maxwell-Boltzmann distribution, according to

$$p_z = \frac{4 \tanh \left[ \frac{\mu B}{2kT} \right]}{3 + \tanh^2 \left[ \frac{\mu B}{2kT} \right]} \quad (6)$$

$$\sim \frac{2}{3} \frac{\mu B}{kT}, \quad (7)$$

where  $\mu$  is the deuteron magnetic moment,  $B$  is the magnetic field,  $k$  is Boltzmann's constant, and  $T$  is the temperature. For typical values of  $B$  (2.5 T) and  $T$  (1 K), the TE polarization is only 0.000 53. A typical TE signal measured during this experiment is shown in Fig. 4(b). The temperature of the target was obtained by averaging the readings of two calibrated resistors in the mixing chamber of the dilution refrigerator. The temperature calibrations of the thermometers were made by comparison with  $^3\text{He}$  and  $^4\text{He}$  vapor pressure measurements to an accuracy of 1%. The magnitude of the magnetic field in the region of the target [required in Eq. (7)] is measured by utilizing the more conventional aspects of the deuteron NMR signal, namely that the NMR center frequency is proportional to the magnetic field strength. In practice, the current in the polarizing magnet is adjusted until the deuteron NMR signal frequency is centered at  $16.650 \pm 0.002$  MHz. This frequency corresponds to a

magnetic field of  $2.4530 \pm 0.000 30$  T.

Once the magnitude of the TE polarization is calculated using Eq. (7), the magnitude of dynamic polarization may be obtained from the ratio of the integrated areas of the dynamic and TE NMR signals. It is straightforward to extract a reliable area for the relatively large dynamic NMR signal (see Fig. 4). The reliability of the integration procedure was checked by assuming different forms (linear or quadratic) for the polynomial fitted to the background underneath the NMR signal. Furthermore, the integration was performed in two ways, either by simply adding the number of counts above the background polynomial, or by fitting the NMR signal with a theoretical line shape. The results were consistent in every case. The background was completely flat, so that the linear fit was used for all the quoted results.

It is much more difficult to integrate the tiny TE signal because the ratio of signal to background is about 3 orders of magnitude smaller than for the dynamic NMR signal. Consequently, a careful determination of the NMR background was made by averaging the measured background on both sides of the NMR signal. This procedure was performed the same way for both the dynamic and the TE NMR signals. The NMR signal is a measure of signal intensity as a function of frequency. The signal intensity is measured as the NMR frequency is swept between about 16.4 and 16.9 MHz. In order to estimate the NMR background in this region, one requires measurements just below and just above these limits in order to avoid the region sensitive to deuteron spin flips. In principle, then, one could merely sweep the NMR frequency in regions just below 16.4 MHz and just above 16.9 MHz. However, the NMR circuit is highly tuned, and in practice it is quite difficult to precisely select all of the tuning parameters (such as the cable length, the tuned circuit and the NMR center frequency, and the phases of the rf signals to the synchronous detector). Slight misadjustments in any of these parameters will not influence the outcome of the TE method, however the results of the asymmetry technique (discussed later) can be influenced by a few percent. Therefore, instead of varying the NMR frequency interval, the deuteron NMR signal was swept out of this frequency interval by adjusting the magnetic field of the target. For this experiment, the NMR background was obtained by averaging measurements obtained at magnetic field strengths 3% above and 3% below the nominal, 2.5 T value. The uncertainty in the integrated area of the TE NMR signal resulting from this procedure was determined by the standard deviation of the measured values obtained at intervals during the course of the experiment, which was typically several weeks long. Each sample consisted of approximately 40 TE measurements.

For a second technique, which does not rely on a measurement of the TE signal, the asymmetry in the peak shape of the dynamically polarized NMR signal was analyzed. This technique, which has been described in Refs. 38 and 39, relies on the fact that the relative intensities of the two peaks in the NMR spectrum are proportional to the intensities of the transitions in the deuteron spin system. Referring to Fig. 4, one peak is proportional to the

$m=0$  to  $m=-1$  transition, and the other to the  $m=+1$  to  $m=0$  transition. The vector polarization may be expressed in terms of the ratio of intensities of the two transitions ( $R$ ) using the relation

$$p_z = \frac{(1-R^2)}{(1+R+R^2)}. \quad (8)$$

The difficulties associated with the asymmetry technique are the determination of  $R$ , and insuring that the effective response to the NMR signal is independent of frequency over the frequency region spanned by the NMR signal. This response was checked by periodically fixing the NMR frequency and sweeping the magnetic field. The asymmetries of the resulting NMR spectra are almost independent of the small uncertainties in tuning and were in good agreement with the results where the rf frequency was swept instead of the magnetic field. The determination of  $R$  is not straightforward because of the complicated shape of the NMR signal. Following the procedure outlined in Ref. 38, a computer program was written which determined  $R$  by fitting the measured deuteron NMR signals to a theoretical line shape.

The validity of these techniques has been confirmed in an independent experiment<sup>39</sup> which measured the target tensor polarization directly by utilizing the known tensor analyzing power  $T_{20}$  at  $90^\circ$  (c.m.) in the  $\pi d \rightarrow 2p$  reaction. In practice, the values of target polarization used in the experiment reported here were obtained from the average of the two (consistent) NMR signal techniques.

## V. RESULTS

The results of this experiment consist of new measurements of  $T_{20}$  at pion bombarding energies of 180, 220, and 256 MeV. At each of these bombarding energies, approximately six angles were obtained. Furthermore, new measurements of  $\tau_{21}$  have also been obtained at 134 and 220 MeV. Approximately twelve angles were obtained at each of the bombarding energies studied in the  $\tau_{21}$  measurements.

These new measurements complement previous ones published by this collaboration. The previous results consist of a twelve-point angular distribution of  $\tau_{21}$  at 180 MeV,<sup>31</sup> as well as six-point angular distributions of  $T_{20}$  at 134 and 151 MeV.<sup>30</sup> Taken as a complete set, the old and new data provide a reasonably complete, systematic measurement of the behavior of the tensor analyzing powers  $T_{20}$  and  $\tau_{21}$  over the range of incident pion energies spanned by the (3,3) resonance. Measurements of these observables at still higher energies, as well as measurements of  $\tau_{22}$ , have been obtained by a group at SIN, and will be presented in a future publication.<sup>34</sup> Planned measurements of several of the spin transfer observables for this reaction would complete the main objectives of experimental study in the fundamental  $\pi d$  system and allow an unambiguous determination of the partial waves for  $\pi d$  scattering. At present, including measurements of the differential cross section,  $iT_{11}$ ,  $T_{20}$ ,  $T_{21}$ , and  $T_{22}$ , only five of the required seven independent observables needed to completely describe  $\pi d$  elastic scattering are measured.

The results of this experiment, together with those acquired previously by this collaboration, are presented in Table I. The new measurements of  $T_{20}$  at  $T_\pi = 180, 220,$  and  $256$  MeV are presented in Fig. 5 along with our earlier results at  $134$  MeV.<sup>30</sup> The data at each bombarding energy consist of six-point angular distributions, confined for the most part to angles greater than about  $\theta_{c.m.} \sim 135^\circ$ . At the higher energies,  $220$  and  $256$  MeV, it was possible to acquire data near  $\theta_{lab} \sim 90^\circ$  because recoil deuterons associated with pions exiting through the split between the polarized target magnet coils were energetic enough to reach the deuteron detectors. All of the measured values of  $T_{20}$  are negative. From Fig. 5 it is apparent that the general trend of  $T_{20}$  in the backward hemisphere is towards increasingly negative values as the bombarding energy is raised from  $134$  to  $256$  MeV. No dramatic changes in the shape of the angular distributions, which in general tend toward more negative values with increasing angle, is observed. In particular, no rapid angular oscillations, such as those seen previously in measurements of the tensor polarization  $t_{20}$  in an experiment at SIN (Ref. 28), are observed at any bombarding energy. The results of that experiment have already been shown to be in error.<sup>30</sup>

A number of measurements of the tensor polarization  $t_{20}$  in  $\pi d$  scattering<sup>25-29</sup> have been published in the last few years. It is possible to compare those results to the

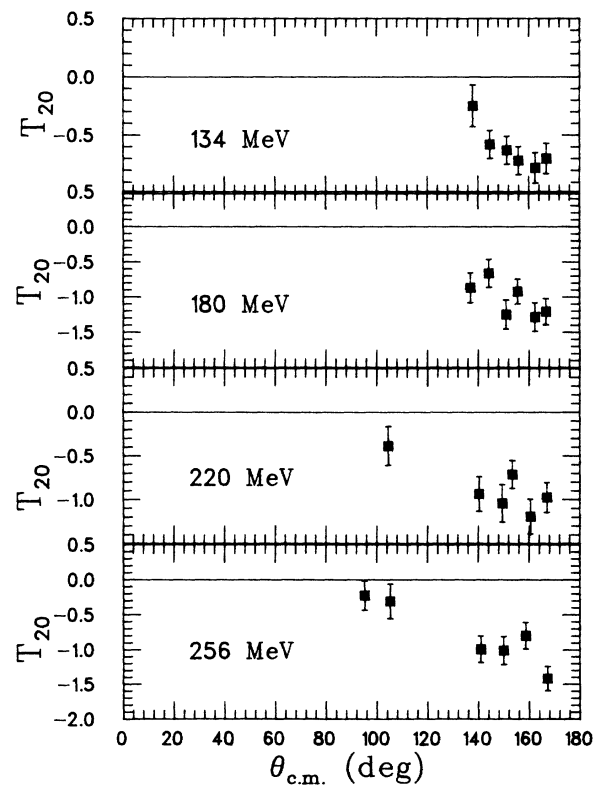


FIG. 5. The angular distributions of  $T_{20}$  measured in this experiment are shown for pion bombarding energies of 180, 220, and 256 MeV. The previously published values at 134 MeV (Ref. 30) are also included.

TABLE I. The results of this experiment are tabulated. In addition, previously published values are tabulated for  $T_{20}$  at 134 and 151 MeV (Ref. 30), as well as for  $\tau_{21}$  at 180 MeV (Ref. 31). The column labeled "Set" distinguishes data acquired in one angular setting of the six detectors from another angular setting.

$T_\pi$ (MeV)	$\theta_{c.m.}$	$\tau_{21}$	$\Delta\tau_{21}$	Set	$T_\pi$ (MeV)	$\theta_{c.m.}$	$T_{20}$	$\Delta T_{20}$	Set
134	126.6	-0.44	0.09	1	134	137.9	-0.25	0.18	1
	136.0	-0.44	0.09	1		144.7	-0.58	0.12	1
	145.3	-0.42	0.09	1		151.4	-0.63	0.12	1
	154.3	-0.48	0.11	1		155.9	-0.72	0.12	1
	163.1	-0.22	0.11	1		162.5	-0.78	0.13	1
	171.3	-0.18	0.10	1		166.9	-0.70	0.13	1
	112.1	-0.32	0.16	2	151	138.2	-0.68	0.19	1
	121.8	-0.37	0.09	2		145.0	-0.75	0.13	1
	131.3	-0.32	0.09	2		151.6	-0.63	0.13	1
	140.7	-0.39	0.08	2		156.0	-0.76	0.13	1
	149.8	-0.50	0.08	2		162.6	-0.84	0.14	1
	158.7	-0.28	0.08	2		167.0	-0.53	0.13	1
180	117.1	-0.38	0.17	1	180	137.0	-0.87	0.21	1
	131.3	-0.57	0.18	1		144.2	-0.66	0.20	1
	140.4	-0.29	0.19	1		151.0	-1.25	0.21	1
	149.4	-0.47	0.18	1		155.6	-0.92	0.18	1
	158.2	-0.37	0.20	1		162.3	-1.29	0.20	1
	126.6	-0.43	0.10	2		166.7	-1.21	0.19	1
	135.9	-0.50	0.10	2	219	104.5	-0.39	0.22	1
	144.9	-0.61	0.14	2		140.3	-0.94	0.20	1
	153.8	-0.40	0.12	2		149.4	-1.04	0.21	1
	162.5	-0.24	0.13	2		153.4	-0.71	0.16	1
	170.8	-0.19	0.21	2		160.5	-1.19	0.20	1
220	122.1	-0.43	0.13	1		167.0	-0.98	0.17	1
	136.0	-0.90	0.21	1	256	95.2	-0.22	0.21	1
	144.9	-0.40	0.21	1		105.3	-0.31	0.25	1
	153.6	-0.74	0.18	1		141.0	-0.99	0.19	1
	162.2	-0.49	0.19	1		149.9	-1.01	0.20	1
	170.5	-0.33	0.18	1		158.6	-0.80	0.19	1
	107.8	-0.27	0.09	2		167.2	-1.42	0.18	1
	117.4	-0.67	0.12	2					
	131.4	-0.69	0.17	2					
	140.4	-0.72	0.15	2					
	149.3	-0.47	0.13	2					
	158.0	-0.57	0.17	2					

results of this experiment. Before doing so, it is useful to summarize the differences between the two observables and the experiments which were performed to measure them.

First of all, in the center-of-mass system the tensor polarization  $T_{20}$ , and the tensor analyzing power  $t_{20}$ , are identical due to time reversal invariance. The former is related to the initial-state deuteron polarization, the latter to the final-state deuteron polarization.  $T_{kq}$  is used to denote tensor analyzing powers, and  $t_{kq}$  to denote tensor polarizations, in accordance with the Madison convention.<sup>32</sup>

As described earlier, a measurement of the tensor analyzing power  $T_{20}$  is a single scattering experiment from a tensor polarized deuteron target. A measurement of the polarization of the final-state deuterons is not required. Instead, the initial-state (target) deuteron polarization is measured using NMR techniques. The measurement is referred to a coordinate system whose  $z$  axis

lies along the direction of the incident pion momentum. Therefore, the laboratory and center-of-mass values of  $T_{20}$  are identical,  $T_{20}(\text{lab})=T_{20}(\text{c.m.})$ .

A measurement of the tensor polarization  $t_{20}$  is performed in a double scattering experiment from an unpolarized (liquid) deuterium target. The polarization of the final-state deuterons is measured in a second scattering [ $^3\text{He}(d,p)^4\text{He}$ ] in a  $^3\text{He}$  cell polarimeter. This measurement is referred to a coordinate system with the  $z$  axis along the direction of the outgoing deuteron momentum. Therefore, the coordinate system is different for every angle measured, and of course the laboratory and center-of-mass values of  $t_{20}$  are not identical,  $t_{20}(\text{lab})\neq t_{20}(\text{c.m.})$ .

In order to compare previous measurements of  $t_{20}(\text{lab})$  to the  $T_{20}(\text{lab}$  or  $\text{c.m.})$  measurements of this experiment, one of two transformations must be performed. Either the published values of  $t_{20}(\text{lab})$  must be transformed to  $t_{20}(\text{c.m.})$ , or the measured  $T_{20}(\text{c.m.})=T_{20}(\text{lab})$  of this experiment must be rotated into the laboratory coordinate

system coinciding with that used for the  $t_{20}$  experiments. We have chosen the latter approach. In either case, the rotation may be performed using the expression

$$t_{20}^{\text{lab}} = \frac{3 \cos^2 \theta - 1}{2} T_{20} + \sqrt{6} \sin \theta \cos \theta T_{21} + \sqrt{3/2} \sin^2 \theta T_{22}, \quad (9)$$

where  $\theta$  ( $\theta > 0$ ) refers to the deuteron recoil angle, and  $T_{kq}(\text{c.m.}) = t_{kq}(\text{c.m.}) = T_{kq}(\text{lab})$ . Unfortunately, the transformation introduces unwanted  $T_{21}$  and  $T_{22}$  components. However, their influence is small in the backward hemisphere where the  $T_{20}$  measurements were performed, due in part to the presence of the  $\sin \theta$  term. In order to make the transformation, we have used calculated values of  $T_{21}$  and  $T_{22}$  from Ref. 7. Specifically, we have used their predictions which omit the  $P_{11}$  term (and, therefore, omit pion absorption), instead of their full calculation, because their calculations without the  $P_{11}$  term do the best job describing the measurements of  $T_{20}$  and  $\tau_{21}$ . No  $T_{22}$  data have been available until now for use in this transformation. A forthcoming publication<sup>34</sup> will, however, provide

these data and, therefore, in the future it will be possible to perform the transformation specified by Eq. (9) using measured values only. The present prescription, which uses calculated values of  $T_{21}$  and  $T_{22}$ , seems reasonable given the small influence of  $T_{21}$  and  $T_{22}$  in the transformation at back angles, the good agreement between measured values of  $\tau_{21}$  and the predicted values used in the transformation, and the corresponding good agreement between the same predictions and the preliminary  $\tau_{22}$  measurements obtained by the SIN collaboration.<sup>34</sup>

The results are shown in Fig. 6. The existing measurements of the tensor polarization  $t_{20}$  are plotted at each of the bombarding energies studied in this experiment, along with the transformed values of  $T_{20}$  measured in this experiment. This figure clearly shows good agreement at all bombarding energies between the projected tensor polarizations of this experiment and the  $t_{20}$  data published previously from double scattering experiments.<sup>25,26,27,29</sup> This agreement is quite significant, given the completely different experimental approaches used for the measurements of  $t_{20}$  and  $T_{20}$ . The only discrepancy arises at 134 MeV, where the results of the double scattering experiments of Ref. 28 (not shown) are in complete disagreement with the results of this (single scattering) experiment, as well as those of the other double scattering experiments.<sup>25,26,27,29</sup> Clearly, the weight of experimental evidence strongly suggests that the results

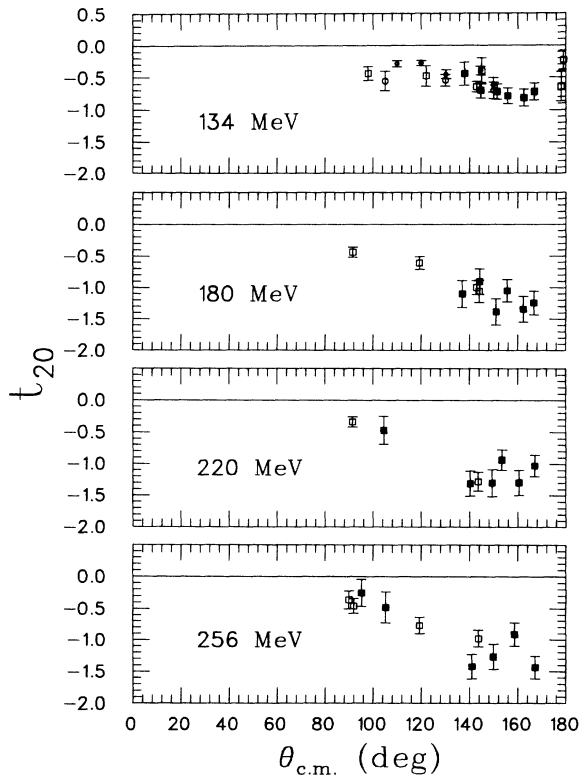


FIG. 6. In this figure the values of  $T_{20}$  measured in this experiment (solid squares), as well as those from Ref. 30 (solid squares at  $T_{\pi} = 134$  MeV), are transformed into tensor polarizations ( $t_{20}$ ) using the expression given by Eq. 9. The results are compared to previous measurements of the tensor polarization  $t_{20}$  from Refs. 25, 26, and 27 (open squares) and Ref. 29 (open circles). The tensor polarization data of Ref. 28, which are known to be error, are not shown (for that reason).

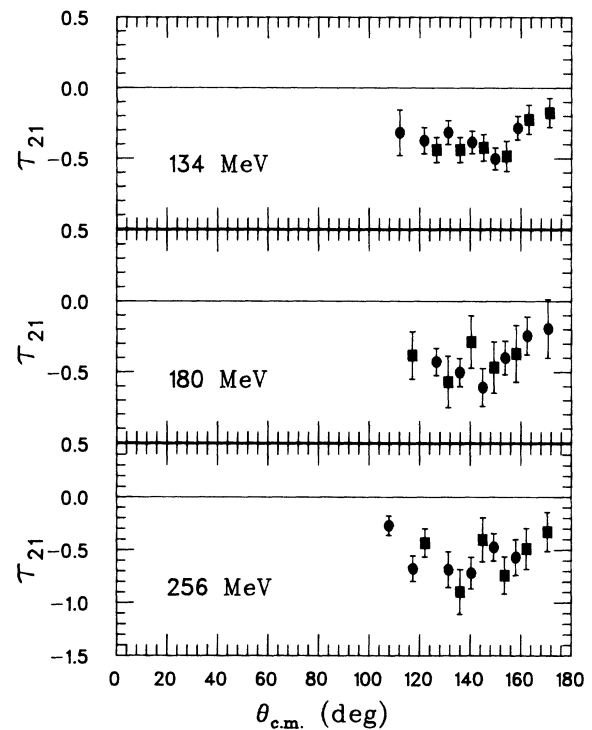


Fig. 7. The angular distributions of  $\tau_{21}$  measured in this experiment are shown for pion bombarding energies of 134 and 220 MeV. The previously published values at 180 MeV (Ref. 31) are also included. Data acquired for different angular settings of the six detectors are distinguished by different symbols.

of Ref. 28 are in error, as pointed out in Ref. 30. At the higher bombarding energies, the only existing  $t_{20}$  measurements are from Ref. 27. Although their results are sparse, good agreement with the present experiment is achieved in every case.

The  $\tau_{21}$  measurements are plotted in Fig. 7. At each of the three bombarding energies studied, the data were collected in two overlapping angular settings of the six detectors. Data acquired in different angular settings are plotted with different symbols in Fig. 7. The consistency obtained with the two angular settings is excellent at each bombarding energy. The range of the angular distributions extends from near  $110^\circ_{\text{c.m.}}$  to about  $170^\circ_{\text{c.m.}}$ . This extensive angular coverage was possible due to the more open geometry associated with the  $45^\circ$  orientation of the polarized target magnet coils. The behavior of  $\tau_{21}$  is similar to that of  $T_{20}$  in that the data are all negative. The angular distributions become more negative as the bombarding energy is raised from 134 to 220 MeV. The angular distributions appear to be smooth.

## VI. THEORETICAL PREDICTIONS

The study of the  $\pi d$  system is important because it is probably the only system in intermediate energy pion physics which can, in principle, be described within an exact, sophisticated theoretical framework. Furthermore, the deuteron is the simplest real nucleus which can be studied with pions, and forms our basis for understanding more complicated systems on a microscopic level. For these reasons, the  $\pi d$  system is certainly the most thoroughly studied pion nucleus system both experimentally and theoretically.

More than a decade of intense research by numerous theoretical groups has led to the development of highly refined three-body calculations employing Faddeev equations to describe the coupled  $\pi NN$  system.<sup>1-14</sup> Here we shall not describe these efforts themselves, but instead we shall refer to their results and compare them to the results of this experiment. For an enumeration and a summary of the differences between the various theoretical camps on this issue, see the short discussion in Ref. 24, or the more thorough treatment in Ref. 40. The ultimate goal of these theoretical efforts is to provide a unified description of all the  $\pi NN$  channels within the framework of a single set of coupled equations. The simultaneous prediction of all measured observables for all  $\pi NN$  channels provides a tight constraint on the theory.

In practice, most of the theoretical effort so far has been focused on the  $\pi d$  elastic and  $pp \rightarrow \pi d$  channels. Experimentalists have responded by providing a broad and diverse data base, especially for these channels, with which to confront the predictions. However, discrepancies between measured and predicted values for even the differential cross section in  $\pi d$  elastic scattering persist to this day. The problem is particularly acute in the backward hemisphere, where the differential cross section is more than 2 orders of magnitude smaller than at the very forward angles. On the one hand, some investigators question the propriety of conclusions drawn from a comparison of measured and predicted spin observables when

problems still exist with the differential cross section. On the other hand, it is the conviction of many others that the detailed comparison of measured and predicted spin observables will provide the clues needed to solve the existing puzzles in the  $\pi d$  system, including perhaps those pertaining to the differential cross section. Failure to predict a given observable implies that at least one amplitude is incorrectly predicted. The influence of a particular amplitude is different for different observables, so it is clear that the best approach is to have measurements of several observables available with which to constrain the amplitudes, and therefore the theory. Spin observables, in particular, may be especially useful due to their sensitivity to the interference of small amplitudes with the larger ones which dominate spin averaged observables like the differential cross section.

Four complex spin amplitudes are required to describe  $\pi d$  elastic scattering, so in principle seven observables need to be measured at each energy and at each scattering angle in order to determine the amplitudes up to a common phase. The data provided by this experiment contribute extensively to two of the required seven observables. In conjunction with previous measurements of the differential cross section and vector analyzing power  $iT_{11}$ , four observables are now available to constrain the theory for a wide range of scattering angles and bombarding energies.

Of the many theoretical predictions available, we have chosen a restricted set with which to make comparisons to the results of this experiment. These include those from the Flinders group,<sup>6-9</sup> the Lyon group,<sup>1-5</sup> the Weizmann group,<sup>10-13</sup> Garcilazo,<sup>14</sup> and the Hannover group.<sup>15</sup> All but the Hannover predictions are three-body, Faddeev calculations which use the same formalism in principle, but differ significantly in several practical aspects. In particular, the methods used to split the  $P_{11}\pi N$  partial-wave input into pole and nonpole parts are quite different among the four Faddeev groups and have a noticeable impact on the ultimate results of the calculations. Although there are several other differences between the various three-body calculations, none has as significant an impact as this particular aspect. For example, the Lyon group has recently added heavy meson exchange to their treatment with only minimal impact on the predictions for the  $\pi d$  elastic scattering observables. Therefore, we focus the bulk of our attention on the  $P_{11}$  problem in the comparison to experiment which follows.

The basic argument used in the treatment of the  $P_{11}$  term by the Flinders, Lyon, and Weizmann groups is that since it is known the pion can be absorbed, there must be a pole near  $E \sim m_n$ , where  $m_n$  is the nucleon mass. In that limit, then, the input  $\pi N$  interaction in the  $P_{11}$  channel must have the form

$$t \rightarrow \frac{f^2}{E - m_n} \equiv t_p, \quad (10)$$

where  $f$  is the dressed  $\pi NN$  vertex and  $t_p$  is the pole term. Then, by definition, the nonpole term is  $t_{\text{np}} = t - t_p$ . Here,  $t$  denotes the on-shell, two-body  $P_{11}$  amplitude, which is very small below about 250 MeV. Physically,

$t_{np}$  describes pion multiple scattering from the two nucleons (without absorption), and  $t_p$  accounts for true absorption. The diagrams for these two processes are shown in Fig. 8. In fact, the arguments leading to the above expressions are much more concise and formal than those presented here. The form given above for the pole term is a consequence of the theory of the  $NN-\pi NN$  system.<sup>1-13,40</sup> For this reason, the Lyon group, the Flinders group, and the Weizmann group all argue that this form must be used regardless of the consequences when comparing to experiment, because it is the only correct form.

Isospin and angular momentum conservation limit the contribution of the pole term exclusively to the  $P_{11}$  channel. In all other channels,  $t_{np}$  is parametrized in terms of one-term separable potentials by fitting to the experimental  $\pi N$  phase shifts.<sup>4,5,7,17</sup> In the  $P_{11}$  channel, both pole and nonpole terms contribute. They are determined as two-term separable potentials fit to the experimental  $\pi N P_{11}$  phase shifts. A two-term potential is required due to the change in sign of the  $P_{11}$  amplitude near 150 MeV. The two potentials are dissimilar, since the pole term must be represented by an attractive potential, and the nonpole term by a repulsive potential. They are correlated in the sense that together, they must add to give the small, overall  $P_{11}$  amplitude. The actual parametrization is constrained by requiring a pole in  $t$  at the nucleon mass, and reasonable values for the scattering volume  $a_{11}$  and the  $\pi NN$  coupling constant, as well as good fits to the  $\pi N$  data including total cross sections. However, there can still be ambiguity in the precise form of the two potentials since the off-shell behavior is not known. Figure 9 shows the experimental  $\pi N P_{11}$  phase shifts<sup>41</sup> as a function of pion bombarding energy, together with the pole and nonpole contributions obtained in a calculation from Ref. 4. Given the fact that the  $P_{11}$  amplitude is so small, it is unfortunate that the pole and nonpole terms are so large, reaching values close to  $90^\circ$  above  $T_\pi \sim 200$  MeV.

The ambiguity in the exact shape of these potentials is overshadowed by another effect on which the results of the calculations are extremely sensitive. The preceding paragraphs have outlined the mechanism for treating the  $P_{11}$ , but have not said why this aspect of the calculations leads to problems. We now come to the heart of the

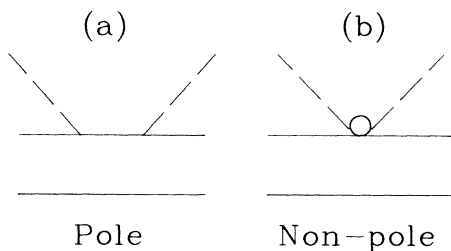


FIG. 8. The diagrams depicting the pole and nonpole terms for the  $P_{11}\pi N$  amplitude are shown. The (a) pole term accounts for true pion absorption. The (b) nonpole term accounts for pion multiple scattering without absorption.

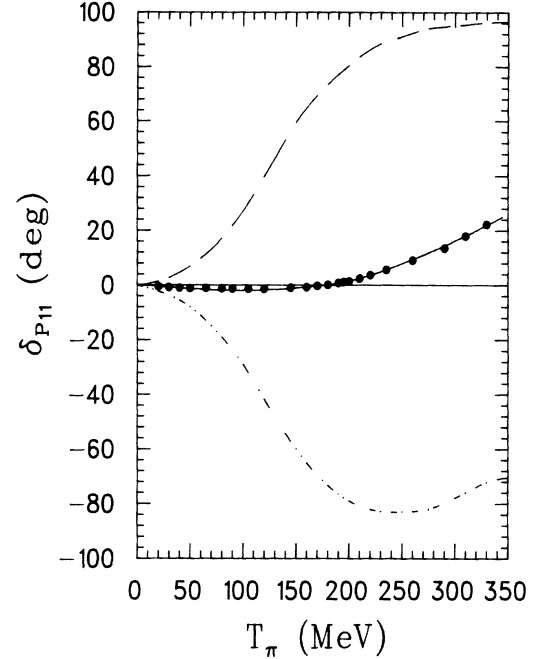


FIG. 9. The experimentally measured values (solid points) (Ref. 41) for the  $P_{11}$  phase shift are plotted in degrees as a function of the pion bombarding energy. The solid curve represents the full  $P_{11}$  amplitude which was fit to these data. The upper (dashed) curve corresponds to the nonpole term parametrization. The lower (dashed-dotted) curve corresponds to the pole term parametrization. The full amplitude consists of the sum of pole and nonpole terms. These potentials were obtained from Ref. 4.

problem. Referring again to Fig. 8, it is clear that for some partial waves, the pole term contribution will be Pauli blocked in the two-nucleon intermediate state. In such cases the nonpole term acts alone and, with no pole term contribution to cancel it, has a considerable impact on the results of the calculations. The Pauli blocking of the  $P_{11}$  pole term is the major source of problems in the theory at the present time.

Garcilazo avoids these problems by using a completely different, controversial splitting which greatly reduces the impact of the pole and nonpole terms. His approach splits  $t$  into two equal halves, then adds and subtracts a term proportional to  $m_n$ ,

$$t = \frac{t(E)(E + m_n)}{2E} + \frac{t(E)(E - m_n)}{2E}. \quad (11)$$

The first term in this expression has a pole near  $(E - m_n)$ , so it is identified as the pole term. The  $(E - m_n)$  factor in the second term of this expression effectively cancels the pole in  $t(E)$  [at  $(E \sim m_n)$ ]. Therefore, this term is identified as the nonpole term. The impact of both terms is negligible since they both contain factors of  $t(E)$  which, as we have shown in Fig. 9, is very small. Its magnitude is less than  $2^\circ$  below pion bombarding energies of about 250 MeV, and so it provides an effective damping mechanism for both pole and nonpole

terms. Therefore, the Pauli blocking of the pole term has almost no influence on the outcome of Garcilazo's predictions.

The Hannover group employs a realistic force model including  $\Delta$ , pion, and nucleon degrees of freedom in a Hamiltonian approach within the framework of noncovariant quantum mechanics. Their model is meant to provide a description of the two-nucleon system below and above pion threshold and its coupled inelastic channels with one pion. This includes  $NN$  elastic scattering, pion absorption and production, and  $\pi d$  elastic scattering. Their model, while not based on Faddeev equations, is particularly interesting since it provides the best description of pion production differential cross sections and spin observables of any of the current theories.

Calculations similar in spirit to those of the Hannover group have been available since 1981 from Betz and Lee at Argonne.<sup>16</sup> The Argonne approach employs a phenomenological Hamiltonian for the interaction of pions, nucleons, and  $\Delta$  isobars. Only the  $P_{33}$   $\pi N$  interaction was considered. Predictions for all four spin observables at pion bombarding energies of 142, 180, 232, and 256 MeV were provided for  $\pi d$  elastic scattering, well in advance of most of the corresponding measurements in this channel. More recently, the model has been extended to describe  $NN$  scattering up to 2 GeV. For clarity in the figures, their results are not reproduced here; rather, we refer the reader to their earlier publication where a thorough presentation can be found.

We now compare the other predictions discussed earlier to the results of this experiment, starting with the measurements of  $T_{20}$ . Figure 10 shows the measured  $T_{20}$  values at 134, 180, 220, and 256 MeV compared to the predictions of the Flinders group, the Lyon group, the Hannover group, the Weizmann group, and Garcilazo. Two sets of predictions are available from the Flinders group. One consists of their full calculation. The other set omits the  $\pi N P_{11}$  input altogether (no absorption and no rescattering) in order to be able to study the influence of this aspect of the calculations.

In the forward hemisphere, all the calculations are in reasonable agreement with one another. In the backward hemisphere, where the  $T_{20}$  measurements were performed, there is much more sensitivity to details of the calculations, and the predictions diverge. The only predictions which are consistent with the data at each bombarding energy are those from Garcilazo, and those from the Flinders group (no  $P_{11}$ ). Given the method discussed earlier which was used by Garcilazo to handle the  $P_{11}$  amplitude, it is not surprising that his calculations are in close agreement with those from the Flinders group in which the  $P_{11}$  was omitted completely. It is surprising that these calculations are in best agreement with the experimental data. The most thorough calculations are from the Lyon group. However, their predictions fail to describe even the shape of the angular distributions of  $T_{20}$  at any energy. In general, they underpredict the experimental results by a wide margin. The Weizmann group overpredicts the data at 134 MeV, and underpredicts the experimental results at the other energies. Their calculations also have an exaggerated angular

structure relative to all the others, in particular near 100°. On the other hand, beyond about 130° their calculations are fairly close to experiment at 134, 180, and 220 MeV. The full calculations from the Flinders group also fail to describe the data. Their full calculations come closest to the data at 180 and 220 MeV, but, in general, have the same pathology as the Lyon calculations elsewhere. The Hannover group represents the only non-Faddeev predictions. They fall in between the two groups of predictions consisting of the Garcilazo and Flinders (no  $P_{11}$ ) predictions, and all the others, at 134 and 220 MeV. At 180 and 256 MeV, however, their predictions seriously underpredict the experimental results.

The consistently better prediction of the data by the two sets of calculations which either leave out or reduce the  $P_{11}$  contribution demonstrates that this aspect of the calculation is the major source of discrepancy between most of the current theories and the experimental data. We now turn our attention to  $\tau_{21}$  to see if this anomaly persists for that spin observable as well.

As described earlier,  $\tau_{21}$  consists of a linear combination of spin observables. Clearly, if the dominant contri-

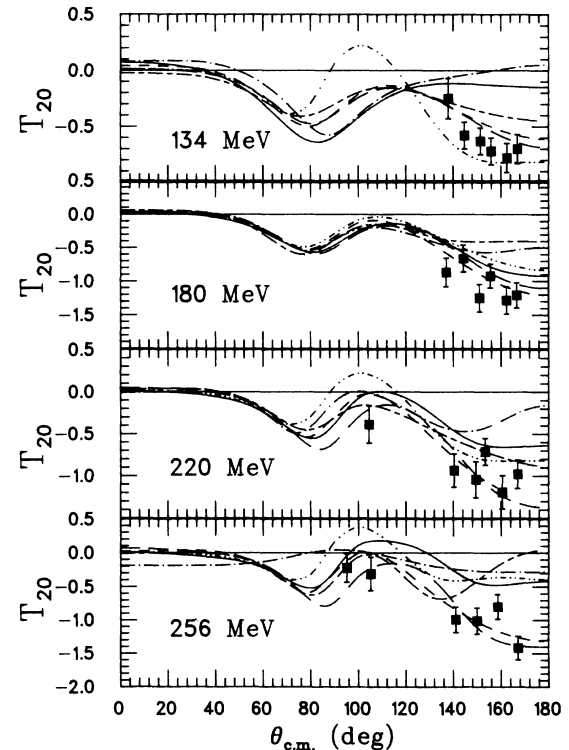


FIG. 10. The measured values of  $T_{20}$  from this experiment and from Ref. 30 are compared to various theoretical predictions for  $T_{\pi} = 134, 180, 220,$  and  $256$  MeV. The predictions of the Flinders group (Ref. 7) are denoted by the solid (full calculation) and dashed (no  $P_{11}$ ) curves. The dashed-dotted curves are from the predictions of the Lyon group (Ref. 5). The predictions of the Weizmann group (Ref. 13) are given by the dash-dot curves, those from Garcilazo (Ref. 14) by the short dashed curves, and those from the Hannover group (Ref. 15) by the long-dash short-dash curves.

bution to  $\tau_{21}$  came from  $T_{20}$ , then little new information would become available from the  $\tau_{21}$  measurements compared to what we already have from the  $T_{20}$  measurements. The experimental geometry for the measurements of  $\tau_{21}$  was adjusted to emphasize  $T_{21}$ . The calculations described earlier provide predictions of  $T_{20}$ ,  $T_{21}$ , and  $T_{22}$ , among others. The predictions for these observables must be combined in the linear combination given by Eq. 4 in order to obtain a prediction for  $\tau_{21}$ , which is the measured quantity. The relative size of each of the terms in Eq. 4 which contributes to  $\tau_{21}$  is shown in Fig. 11 for 134, 180, and 220 MeV, the three bombarding energies at which data were acquired. The predictions of the Flinders group without the  $P_{11}$ , which appear to do the best job describing the  $T_{20}$  measurements outlined earlier, were used in this figure. The figure demonstrates that, in each case, the dominant contribution to  $\tau_{21}$  in the backward hemisphere comes from  $T_{21}$ .

The calculations are compared to the  $\tau_{21}$  data at 134, 180, and 220 MeV in Fig. 12. In contrast to the situation for  $T_{20}$ , the  $\tau_{21}$  predictions are reasonably well clustered, especially at the benchmark bombarding energy of 180 MeV. The full calculations of the Flinders group, and those of the Lyon group are, however, excluded by the

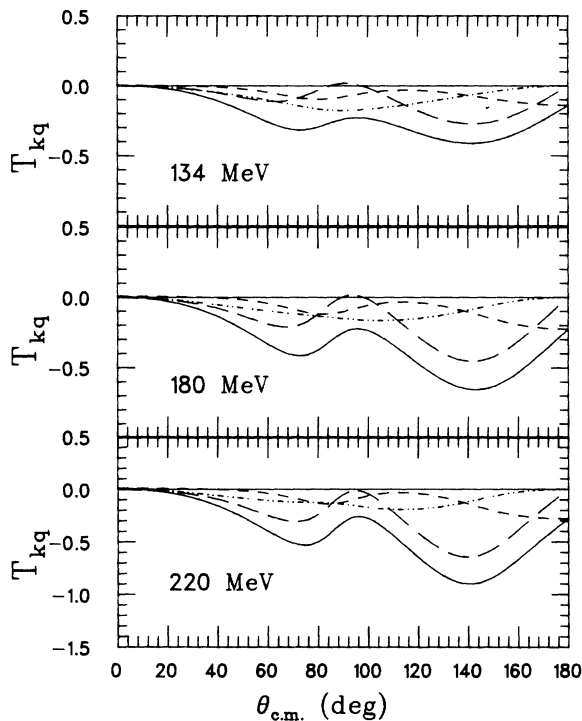


FIG. 11. The contributions of the various terms in the linear combination of spin observables which comprises  $\tau_{21}$  is shown for  $T_{\pi}=134, 180,$  and  $220$  MeV. The terms from Eq. 4 which contribute to the  $\tau_{21}$  predictions are  $T_{22}/2$  (dashed-dot-dot curve),  $T_{20}/2\sqrt{6}$  (short-dashed curve), and  $T_{21}$  (long-dashed curve). The sum of all terms is  $\tau_{21}$  (solid curve). Clearly, the dominant contribution to this observable in the backward hemisphere comes from  $T_{21}$ .

data at 134 MeV. At 180 and 220 MeV, all the predictions fall within the broad band defined by the experimental data, which are of a rather poor quality especially at 220 MeV. Due to a failure of the polarized target, the 220 MeV  $\tau_{21}$  measurements were shorter than planned. Clearly, the comparison of theory and experiment at 134 MeV supports the conclusions drawn earlier for the  $T_{20}$  case. The same at 180 and 220 MeV does nothing to contradict this conclusion.

To summarize, in general the comparison of theory and both the  $T_{20}$  and  $\tau_{21}$  experimental results strongly favors approaches in which the  $P_{11}$  contribution is minimized. There is, apparently, a failure in the theory with respect to this particular aspect. The most sensitive observable to the treatment of the  $P_{11}$  appears to be  $T_{20}$ . The main features of the whole situation can be seen in Fig. 13. This figure is a matrix whose rows denote the pion bombarding energies covered in this experiment (134, 180, 220 and 256 MeV), and whose columns denote all the  $\pi d$  observables which have been measured to date (the differential cross section,  $iT_{11}$ ,  $T_{20}$ , and  $\tau_{21}$ ). The predictions shown in each of the elements of this matrix represent the calculations of the Flinders group, with and without the  $P_{11}$  contribution. The two predictions diverge as the bombarding energy gets farther away from 180 MeV in either direction. Whereas the  $T_{20}$  column stands out strongly favoring the predictions without the  $P_{11}$  as does the 134  $\tau_{21}$  matrix element, the situation is much less clear for the other observables.

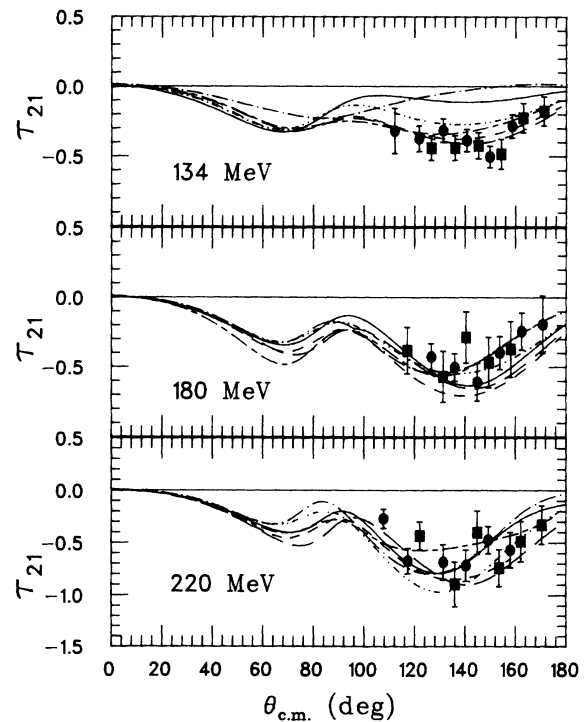


FIG. 12. The measured values of  $\tau_{21}$  from this experiment and from Ref. 31 are compared to various theoretical predictions for  $T_{\pi}=134, 180,$  and  $220$  MeV. The curves have the same meaning as in Fig. 10.

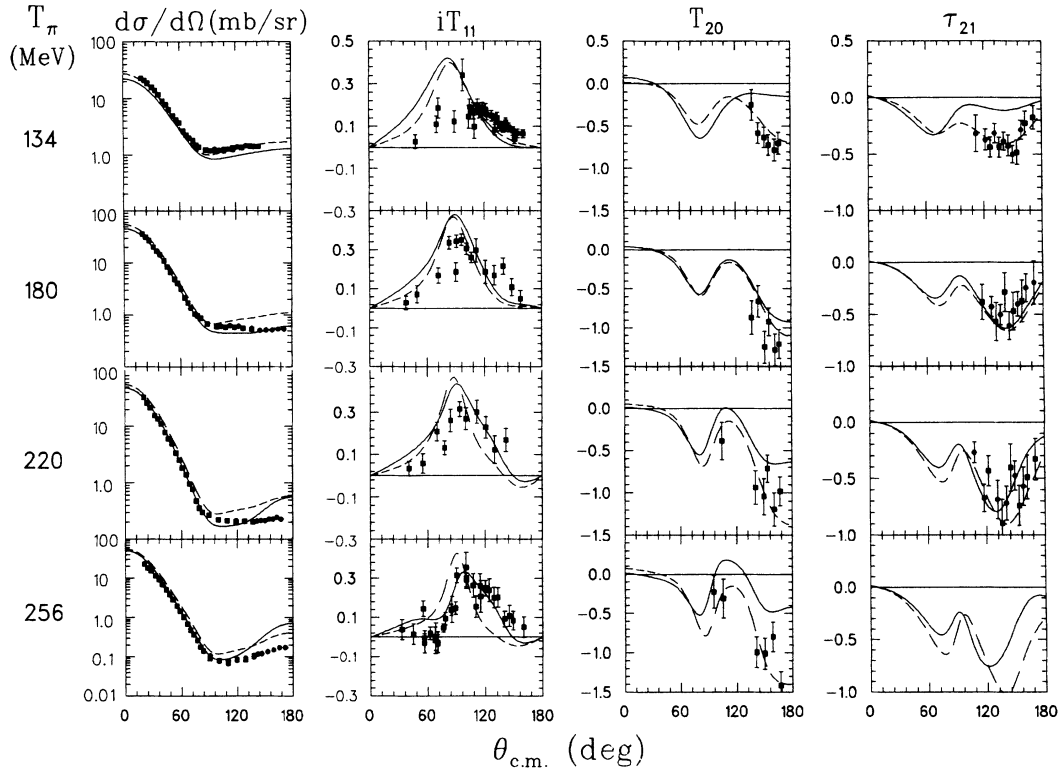


FIG. 13. At each of four representative pion bombarding energies for  $\pi d$  elastic scattering, values of the differential cross section (Refs. 21 and 22),  $iT_{11}$  (Ref. 24),  $T_{20}$  (Ref. 30 and this experiment), and  $\tau_{21}$  (Ref. 31 and this experiment) are shown. The solid curves depict the full three-body predictions of the Flinders group (Ref. 7), and the dashed lines correspond to the same calculations without the  $P_{11}$  contribution.

A number of interesting suggestions have been proposed for dealing with the  $P_{11}$  problem described earlier. Since the heart of the difficulty has to do with the Pauli blocking of the  $P_{11}$  pole term in the two-nucleon intermediate state, some workers have raised the intriguing possibility that there may be a limit to the applicability of the Pauli principle. The nucleon which has absorbed the pion is far off shell, and may no longer be identical to an on-shell nucleon in the sense of the Pauli principle. Were this so, the pole term would not be Pauli blocked and would always largely cancel the nonpole term, eliminating the problem. These speculations are reminiscent of the open question in hypernuclear physics of whether the nonstrange quarks in the hyperon are Pauli blocked in an hypernuclear ground state or not. A more mundane way of stating the problem of the  $P_{11}$  contribution in  $\pi d$  scattering would be to ascribe it to the unknown off-shell behavior of the nucleons in the absorption process.

Recently, Jennings<sup>42</sup> has suggested what may well provide a much more acceptable solution. He has pointed out that there are two diagrams which are left out of the  $P_{11}$  contribution that tend to cancel the diagrams that give rise to the Pauli blocking. Inclusion of the missing diagrams is expected to greatly reduce the problems associated with Pauli blocking in the  $P_{11}$  amplitude. The missing diagrams are crossed diagrams which have two pions simultaneously in the intermediate state, and are, therefore, not explicitly included in the three-body calcu-

lations. Work is presently being carried out to incorporate these diagrams quantitatively into the theory, and to study their influence on the  $\pi d$  observables.

As a final remark we point out the interesting work of Andrade, Ferreira, and Dosch.<sup>43</sup> In a phenomenological approach, they have studied the effects of admixing a short range  $\Delta N$  interaction with the Faddeev amplitudes of Garcilazo. They obtain an excellent fit to the differential cross section and vector analyzing power above 200 MeV where the problems associated with the three-body calculations alone are most severe (see Fig. 13). The agreement achieved is obtained with a four-parameter fit representing the real and imaginary parts of  ${}^5S_2$  and  ${}^5P_3$   $\Delta N$  states. With the new measurements of  $T_{20}$  and  $\tau_{21}$  made available in the present publication, it would be interesting to see what effects the modified amplitudes of Andrade, Ferreira, and Dosch have on these spin observables.

## VII. CONCLUSIONS

We report measurements of the energy dependence of the tensor analyzing powers  $T_{20}$  and  $\tau_{21}$ . Six-point angular distributions of  $T_{20}$  were obtained at bombarding energies of 180, 220, and 256 MeV. Twelve-point angular distributions of  $\tau_{21}$  were obtained at bombarding energies of 134 and 220 MeV. Together with previous measurements of  $T_{20}$  at 134 and 151 MeV,<sup>30</sup> as well as  $\tau_{21}$  at 180

MeV,<sup>31</sup> these data provide a systematic basis for comparison to three-body calculations over the (3,3) resonance region.

Agreement between the present  $T_{20}$  results and the results of previous  $t_{20}$  experiments<sup>25,26,27,29</sup> is good. The only exception is the experiment of Ref. 28, which is inconsistent with all other experiments, including the present one.

The agreement between the present experiment and the preliminary data of Ref. 34 is also good at the single overlapping bombarding energy of 256 MeV, where  $T_{20}$  was measured in both experiments. The exception is a single datum at the most backward angle. The reason for this discrepancy is not known.

The comparison of experiment and theory underscores a failure in the conventional three-body calculations which is most apparent in the observable  $T_{20}$  at several bombarding energies, as well as in  $\tau_{21}$  at 134 MeV. The failure is associated with Pauli blocking effects in the pole term of the  $\pi N P_{11}$  amplitude. In general, the three-

body predictions without pion absorption (no  $P_{11}$ ) provide a satisfactory description of the  $T_{20}$  and  $\tau_{21}$  values measured in the present experiment. In contrast, the full calculations generally fail to describe the data. The most viable solution to this problem has been proposed recently by Jennings and Rinat.<sup>42</sup> It involves the inclusion of missing diagrams in the conventional three-body calculations which tend to cancel the troublesome Pauli blocking of the  $P_{11}$  pole term.

#### ACKNOWLEDGMENTS

We gratefully acknowledge the help of the TRIUMF technical and support staff, as well as the financial support of the Natural Sciences and Engineering Research Council of Canada. This experiment would not have been possible without the considerable skills of the TRIUMF polarized target group. We also thank E. T. Boschitz and B. K. Jennings for many helpful and stimulating discussions during the course of this work.

\*Permanent address: University of Trieste, Trieste, Italy.

<sup>1</sup>Y. Avishai and T. Mizutani, Nucl. Phys. **A326**, 352 (1979); **A338**, 377 (1980); **A352**, 399 (1981); Phys. Rev. C **27**, 312 (1983); G. H. Lamot (private communication).  
<sup>2</sup>C. Fayard, G. H. Lamot, and T. Mizutani, Phys. Rev. Lett. **45**, 524 (1981).  
<sup>3</sup>T. Mizutani, C. Fayard, G. H. Lamot, and S. Nahabetian, Phys. Lett. **107B**, 177 (1981).  
<sup>4</sup>T. Mizutani, C. Fayard, G. H. Lamot, and S. Nahabetian, Phys. Rev. C **24**, 2633 (1981).  
<sup>5</sup>G. H. Lamot, J. L. Perrot, C. Fayard, and T. Mizutani, Phys. Rev. C **35**, 239 (1987).  
<sup>6</sup>I. R. Afnan and B. Blankleider, Phys. Lett. **93B**, 367 (1980); Phys. Rev. C **22**, 1638 (1980).  
<sup>7</sup>B. Blankleider and I. R. Afnan, Phys. Rev. C **24**, 1572 (1981); B. Blankleider (private communication).  
<sup>8</sup>I. R. Afnan and A. T. Stelbovic, Phys. Rev. C **23**, 1324 (1981).  
<sup>9</sup>I. R. Afnan and R. J. McLeod, Phys. Rev. C **31**, 1821 (1985).  
<sup>10</sup>A. W. Thomas and A. S. Rinat, Phys. Rev. C **20**, 216 (1979).  
<sup>11</sup>A. S. Rinat, E. Hammel, Y. Starkand, and A. W. Thomas, Nucl. Phys. **A329**, 285 (1979).  
<sup>12</sup>A. S. Rinat, Y. Starkand, and E. Hammel, Nucl. Phys. **A364**, 486 (1981).  
<sup>13</sup>A. S. Rinat and Y. Starkand, Nucl. Phys. **A397**, 381 (1983); A. S. Rinat (private communication).  
<sup>14</sup>H. Garcilazo, Phys. Rev. Lett. **45**, 780 (1980); Phys. Lett. **99B**, 195 (1981); Phys. Rev. C **26**, 2685 (1982); Phys. Rev. Lett. **53**, 652 (1984); (private communication).  
<sup>15</sup>H. Pöpping and P. U. Sauer, Argonne National Laboratory Report ANL-PHY-83-1, 355 (1983); *Progress in Particle and Nuclear Physics*, edited by A. Faessler (Pergamon, New York, 1986), Vol. 16; *Few Body Problems in Physics*, edited by B. Zeitnitz (North Holland, Amsterdam, 1984); Vol. 2, p. 145; (private communication).  
<sup>16</sup>M. Betz and T.-S. H. Lee, Phys. Rev. C **23**, 375 (1981); T.-S. H. Lee, *ibid.*, **29**, 195 (1984).  
<sup>17</sup>A. W. Thomas, Nucl. Phys. **A258**, 417 (1976).  
<sup>18</sup>J. Arvieux and A. S. Rinat, Nucl. Phys. **A350**, 205 (1980).  
<sup>19</sup>N. Hiroshige, W. Watari, and M. Yonezawa, Prog. Theor. Phys. **68**, 327 (1982).

<sup>20</sup>N. R. Stevenson and Y. M. Shin, Phys. Rev. C **36**, 1221 (1987).  
<sup>21</sup>K. Gabathuler *et al.*, Nucl. Phys. **A350**, 253 (1980).  
<sup>22</sup>C. Ottermann *et al.*, Phys. Rev. C **32**, 928 (1985).  
<sup>23</sup>J. Bolger *et al.*, Phys. Rev. Lett. **46**, 167 (1981); **48**, 1667 (1982).  
<sup>24</sup>G. R. Smith *et al.*, Phys. Rev. C **29**, 2206 (1984).  
<sup>25</sup>R. J. Holt *et al.*, Phys. Rev. Lett. **43**, 1229 (1979).  
<sup>26</sup>R. J. Holt *et al.*, Phys. Rev. Lett. **47**, 472 (1981).  
<sup>27</sup>E. Ungricht *et al.*, Phys. Rev. Lett. **52**, 333 (1984); Phys. Rev. C **31**, 934 (1985).  
<sup>28</sup>J. Ulbricht *et al.*, Phys. Rev. Lett. **48**, 311 (1982); W. Gruebler *et al.*, Phys. Rev. Lett. **49**, 444 (1982); V. Koenig *et al.*, J. Phys. G **9**, L211 (1983); Swiss Institute for Nuclear Research Annual Report NL18, 1984.  
<sup>29</sup>Y. M. Shin *et al.*, Phys. Rev. Lett. **55**, 2672 (1985); N. R. Stevenson *et al.*, submitted to Phys. Rev. C.  
<sup>30</sup>G. R. Smith *et al.*, Phys. Rev. Lett. **57**, 803 (1986).  
<sup>31</sup>G. R. Smith *et al.*, Phys. Rev. C **35**, 2343 (1987).  
<sup>32</sup>*Proceedings of the Third International Symposium on Polarization Phenomena in Nuclear Reactions, Madison, 1970*, edited by H. H. Barschall and W. Haeberli (University of Wisconsin, Madison, 1971).  
<sup>33</sup>P. Schwandt and W. Haeberli, Nucl. Phys. **A110**, 585 (1968).  
<sup>34</sup>C. R. Ottermann *et al.*, submitted to Phys. Rev. C.  
<sup>35</sup>F. Seiler and H. W. Roser, Nucl. Phys. **A315**, 45 (1979); B. A. Robson, *The Theory of Polarization Phenomena* (Clarendon, Oxford, 1974).  
<sup>36</sup>S. Hiramatsu *et al.*, Nucl. Instrum. Methods **160**, 193 (1979).  
<sup>37</sup>G. D. Wait *et al.*, submitted to Nucl. Instrum. Methods.  
<sup>38</sup>K. Guckelsberger and F. Udo, Nucl. Instrum. Methods **137**, 415 (1976); O. Hamada *et al.*, Nucl. Instrum. Methods **189**, 561 (1981).  
<sup>39</sup>G. R. Smith *et al.*, Nucl. Instrum. Methods A **254**, 263 (1987).  
<sup>40</sup>A. W. Thomas and R. H. Landau, Phys. Rep. **58**, 121 (1980).  
<sup>41</sup>R. Koch and E. Pietarinen, Nucl. Phys. **A336**, 331 (1980).  
<sup>42</sup>B. K. Jennings, Phys. Lett. B **205**, 187 (1988); B. K. Jennings and A. S. Rinat, Nucl. Phys. A (in press).  
<sup>43</sup>Sarah C. B. Andrade, E. Ferreira, and H. G. Dosch, Phys. Rev. C **34**, 226 (1986).